Accepted Manuscript

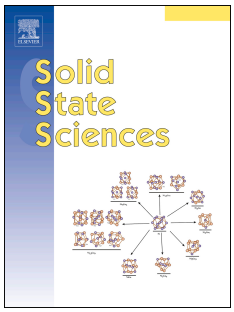

Compressibility, microcalorimetry, elastic properties and EELS of rhenium borides

Christopher Neun, Lkhamsuren Bayarjargal, Dominik Spahr, Felix Schmuck, Wolfgang Morgenroth, Björn Winkler, Benedikt Petermüller, Hubert Huppertz, Victor Milman, Miguel Avalos-Borja, Hector G. Silva-Pereyra

PII: S1293-2558(17)31177-9

DOI: 10.1016/j.solidstatesciences.2018.02.016

Reference: SSSCIE 5642

To appear in: *Solid State Sciences*

Received Date: 1 December 2017

Revised Date: 30 January 2018

Accepted Date: 27 February 2018

Please cite this article as: C. Neun, L. Bayarjargal, D. Spahr, F. Schmuck, W. Morgenroth, Bjö. Winkler, B. Petermüller, H. Huppertz, V. Milman, M. Avalos-Borja, H.G. Silva-Pereyra, Compressibility, microcalorimetry, elastic properties and EELS of rhenium borides, *Solid State Sciences* (2018), doi: 10.1016/j.solidstatesciences.2018.02.016.

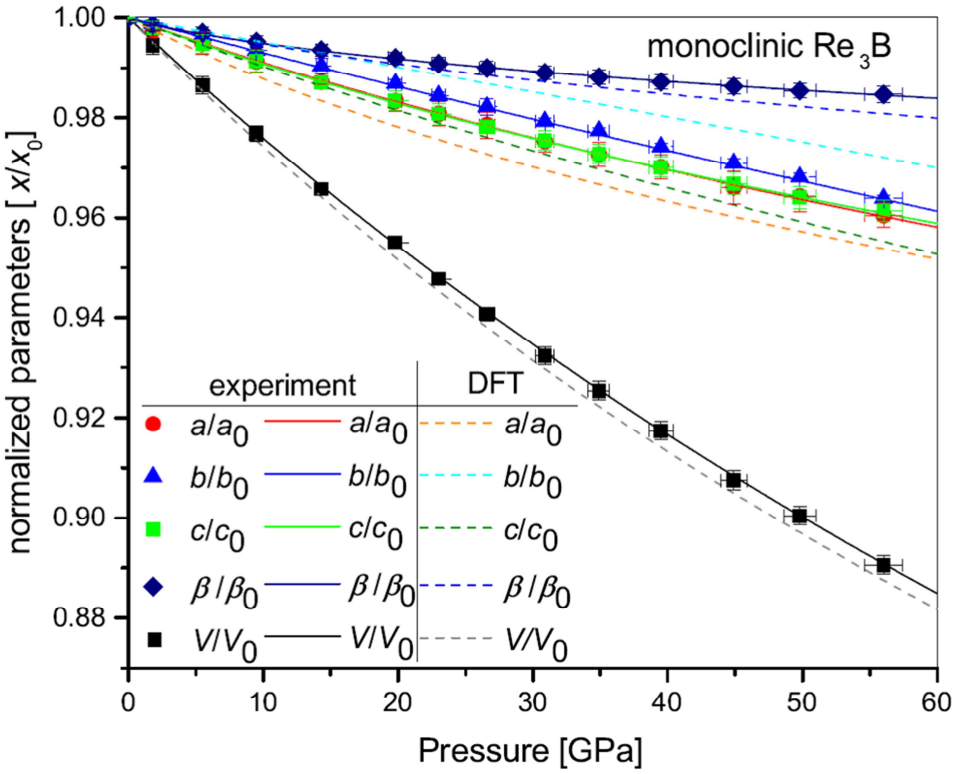

Compressibility, microcalorimetry, elastic properties and EELS of rhenium borides

Christopher Neun,* Lkhamsuren Bayarjargal, Dominik Spahr, Felix Schmuck, Wolfgang Morgenroth, and Björn Winkler
Abteilung Kristallographie, Goethe-Universität Frankfurt

Benedikt Petermüller and Hubert Huppertz
Institut für Allgemeine, Anorganische und Theoretische Chemie, Universität Innsbruck

Victor Milman
Dassault Systèmes BIOVIA, Cambridge, United Kingdom

Miguel Avalos-Borja and Hector G. Silva-Pereyra
Instituto Potosino de Investigación Científica y Tecnológica, IPICYT/División de Materiales Avanzados, San Luis Potosí, S.L.P., México

(Dated: February 28, 2018)

Based on synchrotron X-ray diffraction on phase-pure samples, we revised the bulk moduli of the rhenium borides Re_7B_3 (B_0 (Re_7B_3) = 391(5) GPa) and orthorhombic Re_3B (B_0 (orthorhombic Re_3B) = 393(4) GPa) and determined the bulk modulus of monoclinic Re_3B (B_0 (monoclinic Re_3B) = 390(3) GPa). These results agree well with the DFT calculations on the elastic properties. Microcalorimetry was employed to obtain thermodynamic data for Re_7B_3 and orthorhombic Re_3B and we determined $C_{p,298}$ (Re_7B_3) = 210(4) J/mol, ΔH^0_{298} (Re_7B_3) = 40558(400) J/mol, S^0_{298} (Re_7B_3) = 267(2) J/mol K and $\theta_{D,298}$ (Re_7B_3) = 320(2) K, as well as $C_{p,298}$ (Re_3B) = 86(1) J/mol , ΔH^0_{298} (Re_3B) = 16950(170) J/mol, S^0_{298} (Re_3B) = 112(1) J/mol K and $\theta_{D,298}$ (Re_3B) = 329(3) K. Hardness measurements were performed for Re_7B_3, which gave a Vickers hardness H_V(5 kgf) = 14.5(4) GPa and H_V(10 kgf) = 14.1(3) GPa. Electron energy loss spectroscopy (EELS) was performed on orthorhombic Re_3B and ReB_2, and the experimental spectra are well reproduced by theory in terms of their absorption edges.

Keywords: *Transition metal borides, elastic properties, high-pressure XRD, microcalorimetry, EELS, density functional theory*

INTRODUCTION

Transition metal borides (TM borides) represent a group of potentially high-performance materials with a wide range of interesting physical properties such as high bulk moduli (e.g OsB: 431(23)-453(6) GPa [1]) or high hardness (e.g. WB_4: 46.2(1.2) GPa [1]). This is a large group of compounds as all transition metals from periods 4-6 tend to form binary borides. Only for Cd and Hg no experimental studies have been presented yet [2]. The material properties arise from a combination of the influence of directional bonding, introduced by boron, and the high valence electron density of the metal ions [3]. Hence, for period 6 elements the most promising candidates are the borides of W, Re, Os and Ir and these TM borides have been studied extensively both experimentally and theoretically. Rhenium borides and are well characterized specifically at ambient conditions. In contrast, there are only a few studies at extreme pressure and temperature conditions, most of which are theoretical and primarily concern the diboride (exp: [4],[5],[6],[7],[6], DFT:[8], [9],[10],[11],[12]). In the system Re-B four binary phases have been synthesized, namely ReB_2, Re_7B_3 and Re_3B, which were first described in the early 1960s ([13], [14]) and more recently a new monoclinic modification of Re_3B, which was synthesized at elevated (p,T)-conditions [5]. Among these, ReB_2 attracted the most interest, since it shows a range of interesting properties and can be synthesized at ambient pressure by a large variety of techniques ([7],[15],[16],[17],[18]). Re_7B_3 and Re_3B on the other hand have only been studied with respect to their magnetic properties and their compressibility ([19],[20],[4]).

The crystal structures of the phases investigated in this study are shown in figure 1. Their lattice parameters are listed and compared to results of earlier studies in table I. Atomic positions are listed in table II. The structures of all rhenium boride phases except monoclinic Re_3B have recently been refined using neutron powder diffraction data by Kayhan [21]. Re_7B_3 crystallizes in the acentric hexagonal space group $P6_3mc$ with $Z = 2$ and $a = 7.50(9)$ Å and $c = 4.77(2)$ Å in the Th_7Fe_3 structure type [13]. The boron atoms form isolated planar triangles oriented perpendicular to [001]. ReB_2 shows a centric hexagonal symmetry with space group $P6_3/mmc$ with rhenium on a $2c$ and boron on a $4f$ position [17].

Orthorhombic Re_3B crystallizes in the space group $Cmcm$ with $a = 2.890(1)$ Å, $b = 9.313(4)$ Å, $c = 7.258(3)$ Å and $Z = 4$ [14]. The structure consists of triangular prisms of rhenium in which boron atoms are located at the center ($4c$ position). The monoclinic polymorph of Re_3B shows a slight monoclinic distortion in the bc plane, which

TABLE I. Crystallographic data for rhenium boride phases.

		a [Å]	b [Å]	c [Å]	β [°]	V [Å^3]
ReB_2 ($P6_3/mmc$)	this study, exp.	2.9015(11)	-	7.4798(12)	-	54.53(5)
	[13], exp.	2.900(1)	-	7.475(1)	-	54.44(1)
	[17], exp.	2.9005(5)	-	7.4772(1)	-	54.48(1)
	this study, DFT	2.9008	-	7.4664	-	54.41
	[4], DFT	2.9068	-	7.4878	-	54.79
Re_7B_3 ($P6_3mc$)	this study, exp.	7.5044(11)		4.8776(8)	-	237.88(7)
	[13], exp.	7.50(4)	-	4.77(2)	-	232.4(2)
	[21], exp.	7.5043(1)	-	4.8811(1)	-	238.05(1)
	this study, DFT	7.4859	-	4.8846	-	237.05
	[4], DFT	7.5311	-	4.9018	-	240.77
Re_3B ($Cmcm$)	this study, exp.	2.8898(9)	9.3021(12)	7.2559(11)	-	195.15(9)
	[14], exp.	2.890(15)	9.313(45)	7.258(35)	-	195.35(30)
	[21], exp.	2.8911(1)	9.3156(4)	7.2618(3)	-	195.56(2)
	this study, DFT	2.8839	9.3433	7.2763	-	196.06
	[4], DFT	2.9019	9.3874	7.3278	-	199.62
Re_3B ($C2/m$)	this study, exp.	9.3355(10)	2.8787(11)	7.3047(11)	92.19(5)	196.16(9)
	[5], exp.	9.3636(6)	2.8782(2)	7.3264(5)	92.48(1)	197.26(2)
	this study, DFT	9.4944	2.8548	7.4043	94.09	200.16

lowers the symmetry to $C2/m$. The lattice parameters are $a = 9.3636(6)$ Å, $b = 2.8782(2)$ Å, $c = 7.3264(5)$ Å with a monoclinic angle of $\beta = 92.487(4)°$ [5]. In the study of Tyutyunnik *et al.* [5] it is also stated that monoclinic Re_3B should more precisely be denoted as Re_3B_{1+x}, as there is an additional partial occupation of the $2d$ and $2b$ positions.

In the present study we re-evaluate the bulk moduli of Re_7B_3 and Re_3B, which have been obtained earlier by Juarez-Arellano *et al.* [4]. In that study, Re_7B_3 was found to have an unusually large B_0 value of 438(16) GPa, which almost equals that of diamond and is in the same range as that of other ultra-incompressible phases. The main problem encountered by Juarez-Arellano *et al.* [4] was an excessive overlap of reflections in the diffraction patterns due to the presence of a phase mixture obtained by laser-heating. The presence of additional phases complicated the data analysis and gave rise to large uncertainties in the lattice parameters. In contrast, in the present study phase pure samples were synthesized either via arc-melting or solid state reactions at high temperatures. We also obtained the monoclinic polymorph of Re_3B and compared its properties to the other binary rhenium borides.

Although the structures of orthorhombic Re_3B, Re_7B_3 and ReB_2 have been discovered and solved more than 50 years ago ([13],[14]), an experimental standard entropy has only been published for ReB_2 ([10],[22],[23]). Hence, a second aspect of this study was to obtain further thermodynamic data. Kawano *et al.* [24] found that Re_7B_3 and orthorhombic Re_3B are type-II superconductors with T_c (Re_7B_3) = 3.3 K and T_c (Re_3B) = 4.3 K (respectively 4.7 K by [20]) by resistance and SQUID measurements. Using specific heat measurements performed in a temperature range from 2 to 50 K they established a Debye temperature θ_D (Re_3B) = 600 K, but did not give a value for Re_7B_3, as they were not able to synthesize this compound as a pure phase and observed reflections of ReB_2 as an impurity in their X-ray diffraction measurements. Other thermodynamic parameters like the molar enthalpy and entropy have not been published yet.

Another approach to understand the structure-property relations in rhenium borides is to systematically characterize the interatomic bonding. Hence, this study also includes an investigation of the boron K-edge of Re_3B and ReB_2 by electron energy loss spectroscopy (EELS). The structure of the rhenium borides differ in the boron coordination and the boron-boron interactions and thus were expected to show significant differences in the EEL spectra.

MATERIAL AND METHODS

Synthesis

Re_7B_3 and monoclinic Re_3B were synthesized in a high-frequency (HF) furnace. Rhenium and boron powders in molar ratios of 7:3 and 3:1 were homogenized in an agate mortar for several minutes (Re: powder $\leq$ 10 microns, 99.99 %, ChemPUR Feinchemikalien und Forschungsbedarf, Karlsruhe; B: amorphous powder, technical, 95-97 %, Sigma Aldrich, Steinheim and 99.9 %, ChemPur Feinchemikalien und Forschungsbedarf, Karlsruhe) and annealed for 2 hours at 1973 K in an argon atmosphere.

Orthorhombic Re_3B was synthesized in an arc-melter (MAM-1, E. Bühler GmbH, Hechingen) by melting the elements with varying amounts of excess boron (0 - 20 weight percent). The powders were mixed in an agate mortar and pressed into pellets of five mm diameter. Prior to the arc melting experiments, a titanium getter was molten to absorb any remaining traces of oxygen from the atmosphere.

ReB_2 was synthesized in a multi-anvil press with a Walker-type module. The powder was inserted into a crucible made of hexagonal boron nitride (HeBoSint P100, Henze BNP GmbH, Kempten, Germany), and placed

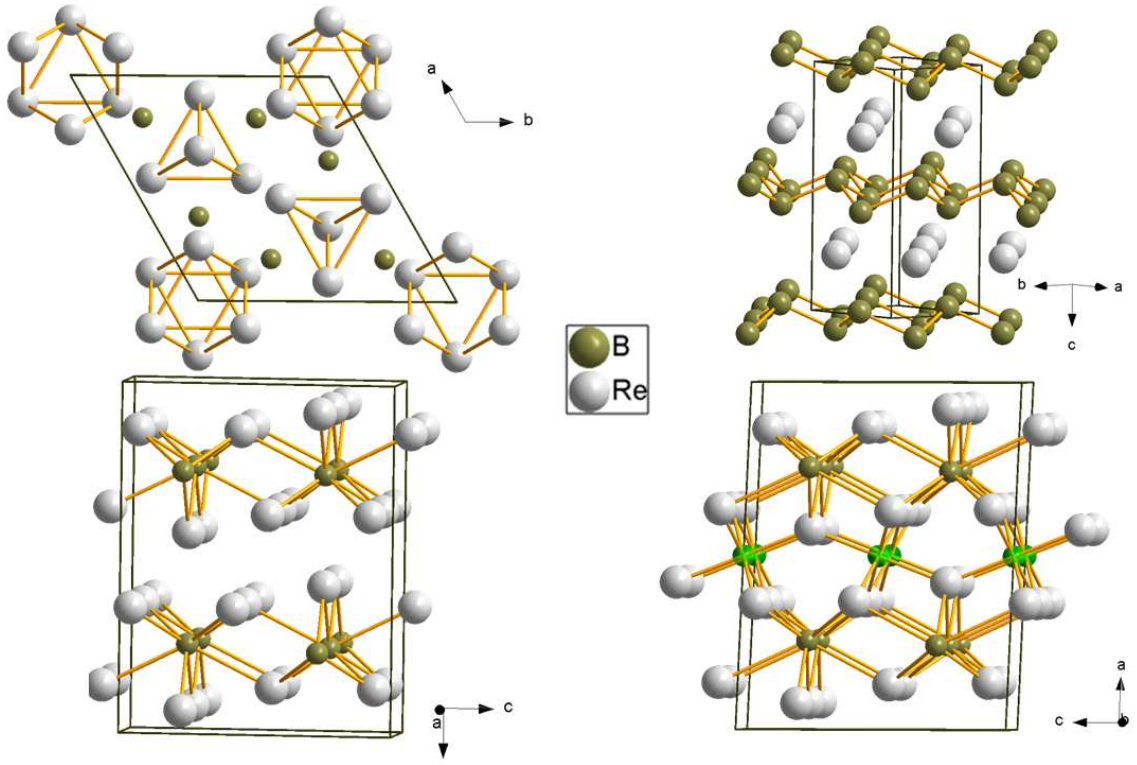

FIG. 1. Structures of Re_7B_3 (top left), ReB_2 (top right) and the two Re_3B polymorphs [13] (bottom left: orthorhombic Re_3B, bottom right: monoclinic Re_3B with the additional partially occupied sites marked in light green [5]).

TABLE II. Structural parameters of the investigated rhenium boride phases.

compound	atom	Wyckoff symbol	site symmetry	x	y	z	site occupancy
ReB_2							
from[17]	Re	$2c$	$\bar{6}m2$	1/3	2/3	1/4	1
	B	$4f$	$3m$	1/3	2/3	0.5496	1
Re_7B_3							
from [13]	Re	$2b$	$3m$	1/3	2/3	0.068	1
	Re	$6c$	m	0.122	0.878	1/4	1
	Re	$6c$	m	0.544	0.456	0.068	1
	B	$6c$	m	0.813	0.187	0.330	1
orthorhombic Re_3B							
from [14]	Re	$8f$	m	0	0.135	0.062	1
	Re	$4c$	$m2m$	0	0.426	1/4	1
	B	$4c$	$m2m$	0	0.744	1/4	1
monoclinic Re_3B							
from [5]	Re	$4i$	m	0.135	0	0.072	1
	Re	$4i$	m	0.870	0	0.559	1
	Re	$4i$	m	0.423	0	0.244	1
	B	$4i$	m	0.744	0	1/4	1
	B	$2d$	$2/m$	1/2	0	1/2	$x \leq 1$
	B	$2b$	$2/m$	0	1/2	0	$x \leq 1$

inside a 14/8 assembly. The assembly was compressed to 12.5 GPa within four and a half hours by a high-pressure device consisting of a hydraulic 1000 t press (Mavo Press LPR 1000-400/50, Max Voggenreiter GmbH, Mainleus, Germany) and a Walker-type module (Max Voggenreiter GmbH) with eight tungsten carbide cubes (HA-7%Co, Hawedia, Marklkofen, Germany). The mixture was heated from ambient temperature to 1473 K within five min. The temperature was held for 30 minutes and afterwards reduced to 973 K in one hour. After decompression, the sample was extracted from the surrounding assembly parts by mechanical separation. A more detailed description of this setup can be found in the literature ([25],[26]).

X-ray diffraction

X-ray diffraction experiments were performed using a X'Pert Pro diffractometer (PANalytical) using Cu-$K_{\alpha 1}$ radiation in Bragg-Brentano geometry and a STOE STADI

P powder diffractometer (Bruker) using Mo-$K_{\alpha 1}$ radiation in transmission geometry. Samples were thoroughly ground either in an agate or tungsten carbide mortar beforehand. Diffractometer parameters were determined by measuring a silicon standard of 99.999 % purity. In Bragg-Brentano geometry all diffraction patterns were collected using an oriented silicon single-crystal plate. The patterns measured in transmission geometry were collected from samples placed between 2 foils of polyvinyl acetate, which were then mounted on a sample holder. For data refinement we employed the GSAS [27], EXPGUI [28] and TOPAS [29] software packages and carried out both Le Bail and Rietveld refinements.

In our high-pressure experiments, we used Boehler-Almax type diamond anvil cells [30], which where loaded with Ne as pressure-transmitting medium. Samples were placed in holes of 110 - 130 µm in diameter, which were drilled by a custom-built laser lathe in pre-indented Re gaskets (40 - 50 µm in thickness). The pressure was determined using the ruby fluorescence method [31].

Synchrotron X-ray diffraction experiments at high pressures were performed at the beamline P02.2 of the PETRA III synchrotron (DESY, Hamburg, Germany). The diffraction patterns were acquired with a Perkin Elmer XRD1621 detector at wavelengths of 0.2907 and 0.2945 Å with beams focused to 1.5 by 2.3 µm FWHM by Kirkpatrick-Baez mirrors. In order to improve the sampling statistics, samples were rotated by 20° during the 10 s data acquisition time. A CeO_2 standard was used to determine the sample-to-detector distance and for detector calibration during the experiments. The diffraction patterns were corrected and integrated using the FIT2D and DIOPTAS software packages ([32] [33]).

Determination of the compressibility

The compressibilities were determined by investigating the dependence of the unit cell parameters upon compression which were obtained by Le Bail refinements. The data were fitted using a third order Birch-Murnaghan (BM) equation of state ([34],[35]) using the EosFit software package [36]:

$$p(V) = \frac{3B_0}{2}\left[(\frac{V_0}{V})^{\frac{7}{3}} - (\frac{V_0}{V})^{\frac{5}{3}}\right]\left[1+\frac{3}{4}(B_0'-4)\left[(\frac{V_0}{V})^{\frac{2}{3}}-1\right]\right] \quad (1)$$

with $B_0' = \left(\frac{\partial B}{\partial p}\right)_{p=0}$. Here p is the pressure, V_0 is the volume at ambient conditions, V is the unit cell volume at the respective pressure and B_0 is the bulk modulus. In the second order BM equation of state, B_0' is constrained to 4.

Microcalorimetry

Microcalorimetry was performed using a Quantum Design thermal relaxation calorimeter (Physical Properties Measurement System, Quantum Design). Compacted, polycrystalline fragments of the samples were prepared so that one flat and polished surface was present to guarantee a good thermal coupling of the sample to the sample holder. Powdered samples were thoroughly ground in a tungsten carbide mortar to reduce pores and encapsuled in a copper container (Alfa Aesar, 99.999 %). In this case, the heat capacity of copper had to be subtracted afterwards. We have shown the accuracy of our measurements to be 1% in the temperature region between 40 and 300 K, and 2% below 40 K by comparing the measurement of a standard material (Cu, Alfa Aesar, 99.999 %) with the values obtained in [37]. In both setups the samples were mounted using Apiezon-N grease. All samples weighed between 10 and 25 mg and were measured in the temperature range between 1.8 and 395 K at 150 different temperatures. The temperature steps were reduced logarithmically from 395 to 1.8 K. At each step, the heat capacity was measured three times by the relaxation method using the two-τ model ([38], [39]).

Neglecting the difference between C_p and C_V, the Debye temperature θ_D can be determined using

$$C_V = \frac{12\pi^4}{5} nR\left(\frac{T^3}{\theta_D}\right) \quad (2)$$

where n is the number of atoms per unit cell and R = 8.31446 J $mol^{-1}K^{-1}$ [40]. In the temperature range between 0 and 298.15 K, the molar entropy S^0 and the molar enthalpy ΔH were calculated from the equations

$$\Delta H = \int_0^{298.15} C_p \; dT \quad (3)$$

and

$$S^0 = \int_0^{298.15} \frac{C_p}{T} \; dT \quad (4)$$

[40] by integrating the measured data numerically.

Hardness measurements

Hardness measurements were performed by the Vickers method using a Mitutoyo Hardness Testing Machine (Mitutoyo America Corporation, Illinois). Here, we used a pyramid-shaped diamond indenter with an apex angle

of 136°. Given this geometry, the Vickers hardness H_V can be calculated by

$$H_V = 2\ \sin(\phi)\ \frac{gL}{2a} = 1854.4\ \frac{F}{2a}\ , \qquad (5)$$

with ϕ as apex angle of the diamond indenter (°), g as the gravitational acceleration (m/s^2), L as the indentation load (kg), a as the average indentation diagonal (μm) and F as the indentation load (N).

The sample used for hardness determination was ground to a thickness of 2 mm using diamond coated polishing disks (160 mesh, GRAVES Company, Pompano, Florida). Surface polishing was carried out using diamond paste with decreasing grain sizes of 15, 10, 5, 3 and 1 μm (Karl Fischer GmbH, Pforzheim).

Density functional theory calculations

In order to obtain a better understanding of the structure-property relations of the synthesized compounds, we performed density functional theory (DFT) calculations employing the CASTEP code [41]. This code implements the Kohn-Sham DFT based on a plane wave basis set in conjunction with pseudopotentials. The plane wave basis set is unbiased (as it is not atom-centered) and does not suffer from basis set superposition errors in comparison to atom-centered analogues. It also makes converged results straightforward to obtain in practice, as the convergence is controlled by a single adjustable parameter, the plane wave cut-off, which was set to 390 eV. All pseudopotentials were ultrasoft and were generated using the WC-GGA to allow for a fully consistent treatment of the core and valence electrons [42]. Brillouin zone integrals were performed by implementing Monkhorst-Pack grids with spacings of less than 0.028 Å^{-1} between individual grid points. A simultaneous optimization of the unit cell parameters and internal coordinates was performed in the way that forces were converged to 0.005 eV/Å and the stress residual to 0.005 GPa. Elastic stiffness coefficients, c_{ij}, were derived by stress-strain calculations. In order to investigate the monoclinic polymorph of Re_3B, in which some boron atoms are located on partially occupied sites, supercell calculations were carried out from which the structures and energies of numerous configurations were obtained with "excess" boron.

Electron energy loss spectroscopy (EELS)

Samples used for EELS measurements were mechanically ground in an agate mortar beforehand to obtain very small particles. Afterwards the grains were treated in an ultrasonic bath with isopropyl alcohol to separate them. They were then mounted on lacey carbon coated copper grids.

The EEL spectra were acquired with a FEI Tecnai F30 transmission electron microscope equipped with a Gatan image filter (GIF). The voltage used was 300 kV. The background was subtracted from all EEL spectra with the Gatan Digital Micrograph software by using a power law fitting model.

RESULTS

Phase analysis

We obtained high quality samples of orthorhombic Re_3B, Re_7B_3 and ReB_2 with no or only minor amounts of impurity phases. All of them could be synthesized either by arc-melting, by annealing in a multi-anvil press or using a HF furnace. The Rietveld refinement of Re_7B_3 is shown in figure 2. There are no impurity phases detectable by conventional X-ray diffraction for Re_7B_3 synthesized in a HF furnace. In the case of orthorhombic Re_3B, phase pure samples can be obtained by arc-melting a sample with a Re:B ratio of 3:1, either using no excess or an excess of up to 5 wt.-% of boron. An excess of 10 wt.-% and more leads to the additional formation of Re_7B_3. The Rietveld refinement of the sample obtained without excess boron is shown in figure 3.

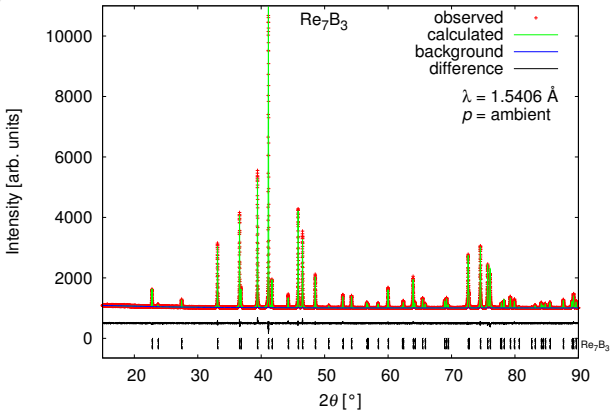

FIG. 2. Rietveld refinement of Re_7B_3. The Bragg positions are represented by tickmarks.

Monoclinic Re_3B was obtained in conjunction with small amounts of orthorhombic Re_3B by heating powders with a molar ration of 3:1 in a HF furnace at 1973 K and ambient pressure. This is a new result, since this polymorph was up to now only synthesized at elevated pressures ($p = 10$ GPa) and high temperatures ($T = 2073$ K) by Tyutyunnik *et al.* [5]. The Rietveld refinement is shown in figure 4. ReB_2 was synthesized in a multi-anvil apparatus at 12.5 GPa and 1473 K from powders of the elements after mixing them carefully in an agate mortar.

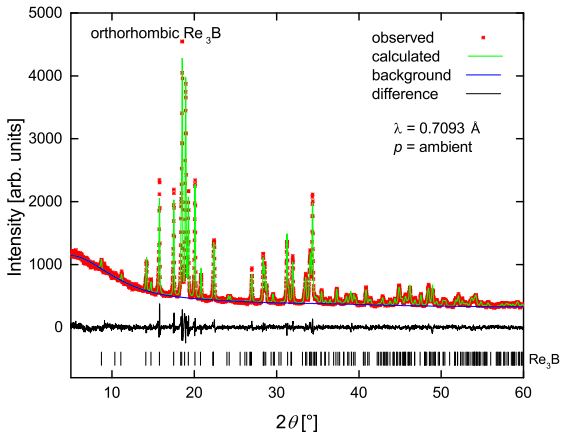

FIG. 3. Rietveld refinement of orthorhombic Re_3B. There are no indications of any impurity phases. The Bragg positions are represented by tickmarks

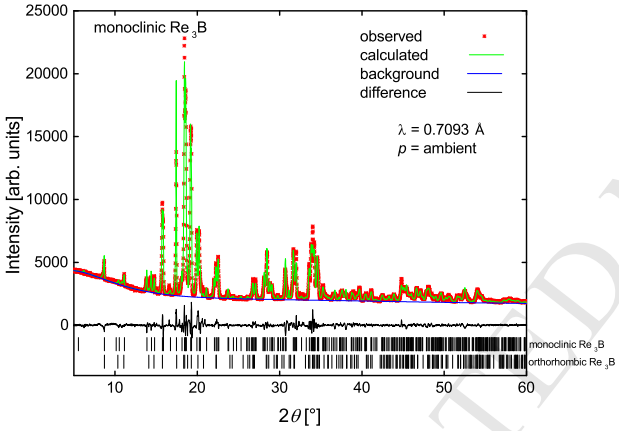

FIG. 4. Rietveld refinement of monoclinic Re_3B. Orthorhombic Re_3B is present as an impurity phase in small amounts. The Bragg positions of both phases are represented by tickmarks

The Rietveld refinement of ReB_2 is shown in figure 5. The lattice parameters of the four rhenium borides are listed and compared to other studies in table I.

Compressibility from diffraction data at high pressures

For Re_7B_3 we determined the equation of state up to a pressure of 42 GPa (figure 6). We did not observe a structural phase transition upon pressure increase. The experimentally obtained bulk modulus is $B_0 = 391(5)$ GPa with $B_0' = 4.9(3)$. The compression behavior of the lattice parameters is shown in table III.

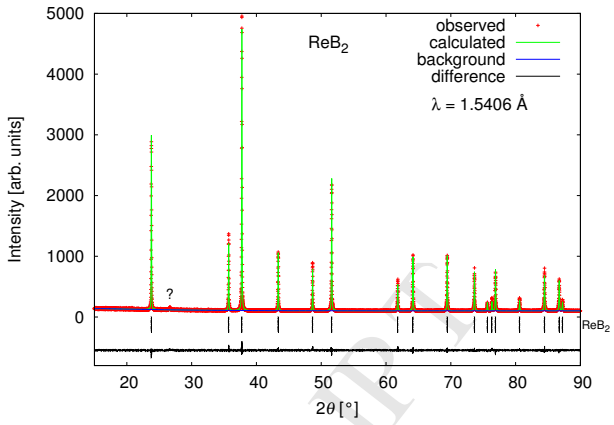

FIG. 5. Rietveld refinement of ReB_2. One small reflection at approximately 27° 2θ could not be assigned to any phase.

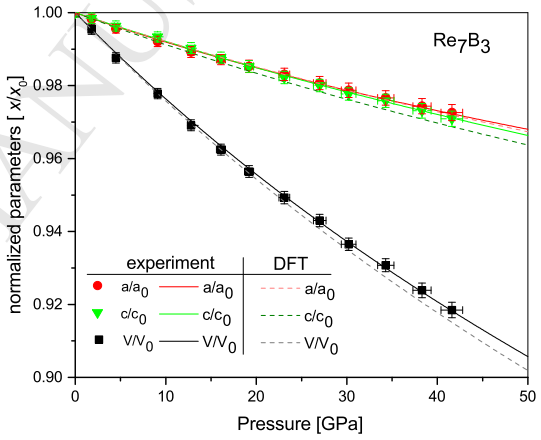

FIG. 6. Pressure dependence of the Re_7B_3 lattice parameters up to 50 GPa (experimental data up to 42 GPa). Fitting a third order BM equation of state (solid lines) yielded a bulk modulus of 391(5) GPa with a pressure derivative of 4.9(3). Both values are in good agreement with the results obtained from fitting the DFT data (dashed lines).

Orthorhombic Re_3B also did not show a structural transformation up to 32 GPa (see figure 7). Fitting a 3^{rd} order BM equation of state to the data yielded $B_0 = 393(4)$ GPa with $B_0' = 2.8(2)$. The pressure dependence of the lattice parameters is listed in table IV.

Monoclinic Re_3B was investigated up to a pressure of 56 GPa, which is shown in figure 8. No structural phase transition was observed. We obtained $B_0 = 390(3)$ GPa and $B_0' = 3.8(2)$. The compression behavior of the lattice parameters is listed in table V.

TABLE III. Pressure dependence of the unit cell parameters for Re_7B_3 derived both experimentally and from DFT-GGA model calculations.

p [GPa]		a [Å]	c [Å]	V [Å^3]
0	exp.	7.5404(9)	4.8776(8)	237.83(5)
0	DFT	7.4859	4.8846	237.05
1.8(1)	exp.	7.4908(13)	4.8695(16)	236.71(11)
4.5(1)	exp.	7.4705(14)	4.8591(18)	234.85(11)
9.1(2)	exp.	7.4445(14)	4.8445(16)	232.52(12)
10	DFT	7.4271	4.8419	231.31
12.8(2)	exp.	7.4228(15)	4.8295(15)	230.45(14)
16.1(2)	exp.	7.4070(17)	4.8170(19)	228.87(15)
19.2(3)	exp.	7.3930(18)	4.8050(18)	227.44(14)
20	DFT	4.3743	4.8035	226.22
23.1(4)	exp.	7.3767(17)	4.7903(18)	225.74(16)
27.0(5)	exp.	7.3587(19)	4.7795(21)	224.25(16)
30	DFT	7.3264	4.7688	221.67
30.2(5)	exp.	7.3439(22)	4.7681(23)	222.70(18)
34.3(6)	exp.	7.3281(22)	4.7591(22)	221.33(17)
38.3(6)	exp.	7.3111(21)	4.7457(24)	219.67(19)
40	DFT	7.2823	4.737	217.55
41.6(7)	exp.	7.2981(22)	4.7351(25)	218.41(22)
50	DFT	7.2823	4.7075	213.78

TABLE IV. Pressure dependence of the unit cell parameters for *Cmcm* Re_3B derived both experimentally and from DFT-GGA model calculations.

p		a [Å]	b [Å]	c [Å]	V [Å^3]
0	exp.	2.8898(9)	9.3021(12)	7.2559(11)	195.15(9)
0	DFT	2.8839	9.3433	7.2763	196.06
2.2(1)	exp.	2.8825(11)	9.2850(15)	7.2450(13)	193.91(12)
4.8(2)	exp.	2.8740(12)	9.22602(16)	7.2350(12)	192.55(13)
9.1(2)	exp.	2.8624(14)	9.2330(16)	7.2130(15)	190.63(15)
10	DFT	2.8614	9.2696	7.2136	191.34
11.8(3)	exp.	2.8580(15)	9.2131(17)	7.1951(17)	189.45(16)
15.6(3)	exp.	2.8498(14)	9.1901(19)	7.1781(17)	187.98(18)
18.3(3)	exp.	2.8418(14)	9.1719(16)	7.1676(16)	186.82(16)
20	DFT	2.8409	9.2037	7.1581	187.16
23.7(4)	exp.	2.8312(14)	9.1411(16)	7.1341(19)	184.64(17)
28.4(4)	exp.	2.8195(15)	9.1101(19)	7.1050(17)	182.50(17)
30	DFT	2.8222	9.1435	7.1089	183.44
31.5(6)	exp.	2.8128(17)	9.0832(22)	7.0970(20)	181.37(20)

TABLE V. Pressure dependence of the unit cell parameters for monoclinic Re_3B derived both experimentally and from DFT-GGA model calculations.

p [GPa]		a [Å]	b [Å]	c [Å]	V [Å^3]	β [°]
0	exp.	9.3355(10)	2.8787(11)	7.3047(11)	196.16(9)	92.19(5)
0	DFT	9.4944	2.8548	7.4034	200.16	94.09
1.8(1)	exp.	9.3121(12)	2.8755(11)	7.2895(12)	195.06(12)	92.05(6)
5.5(2)	exp.	9.2880(13)	2.8685(11)	7.2666(13)	193.52(12)	91.91(6)
9.5(3)	exp.	9.2545(15)	2.8601(14)	7.2417(17)	191.62(15)	91.75(5)
10	DFT	9.3704	2.8434	7.3294	194.92	93.50
14.3(4)	exp.	9.2159(11)	2.8511(11)	7.2102(12)	186.82(12)	91.59(7)
19.8(5)	exp.	9.1801(13)	2.8411(12)	7.1837(13)	187.34(13)	91.45(7)
20	DFT	9.2864	2.8265	7.2655	190.41	93.21
23.0(5)	exp.	9.1559(15)	2.8341(13)	7.1643(17)	185.90(16)	91.35(8)
26.6(6)	exp.	9.1354(15)	2.8275(13)	7.1450(15)	184.53(14)	91.27(7)
30	DFT	9.2134	2.8111	7.2059	186.40	92.92
30.9(7)	exp.	9.1052(16)	2.8191(15)	7.1257(16)	182.89(16)	91.18(7)
34.9(8)	exp.	9.0808(17)	2.8136(14)	7.1057(16)	181.53(16)	91.10(7)
39.5(9)	exp.	9.0569(18)	2.8045(15)	7.0862(7)	179.97(17)	91.01(7)
40	DFT	9.1483	2.7969	7.1515	182.79	92.67
44.9(1.0)	exp.	9.0186(19)	2.7951(17)	7.0625(18)	178.02(18)	90.93(8)
49.8(1.2)	exp.	9.0832(17)	2.8128(21)	7.0970(20)	176.64(20)	90.85(8)
50	DFT	9.0891	2.7841	7.0997	179.45	92.38
55.8(1.4)	exp.	8.9967(21)	2.7747(19)	7.0226(21)	174.69(20)	90.78(8)

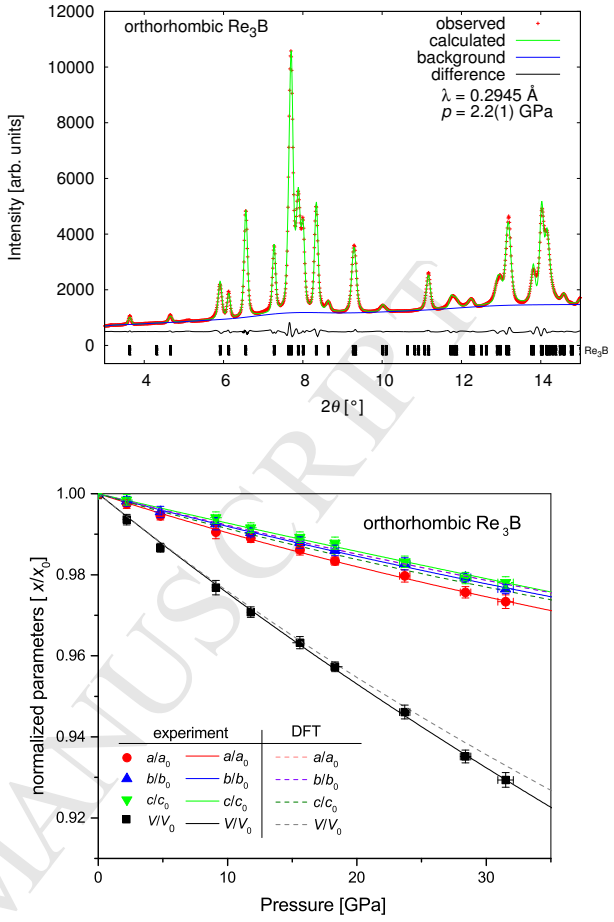

FIG. 7. *Top*: Le Bail refinement of the synchrotron diffraction pattern of orthorhombic Re_3B at 2.2(1) GPa. There are no indications of an impurity phase. *Bottom*: Pressure dependence of the lattice parameters up to 32 GPa. Fitting a third order BM equation of state (solid lines) yielded a $B_0 = 393(4)$ GPa and $B_0' = 2.8(2)$. The experimentally determined pressure dependence of the lattice parameters agrees well with the DFT results.

TABLE VI. Compressibilities of this study compared to previous findings

compound	space group	BM order	method	B_0 [GPa]	B'	reference
Re_7B_3	$P6_3mc$	3^{rd}	exp.	391(5)	4.9(3)	this study
		2^{nd}	exp.	438(16)	-	[4]
		3^{rd}	DFT	386(1)	4.4(2)	this study
		-	DFT	380	-	[43]
		-	DFT	385(1)	-	[4]
Re_3B	$Cmcm$	3^{rd}	exp.	393(4)	2.8(2)	this study
		2^{nd}	exp.	320(15)	-	[4]
		3^{rd}	DFT	389(1)	4.4(2)	this study
		-	DFT	420	-	[43]
		-	DFT	389(1)	-	[4]
Re_3B	$C2/m$	3^{rd}	exp.	390(3)	3.8(2)	this study
		3^{rd}	DFT	362(1)	4.4(3)	this study

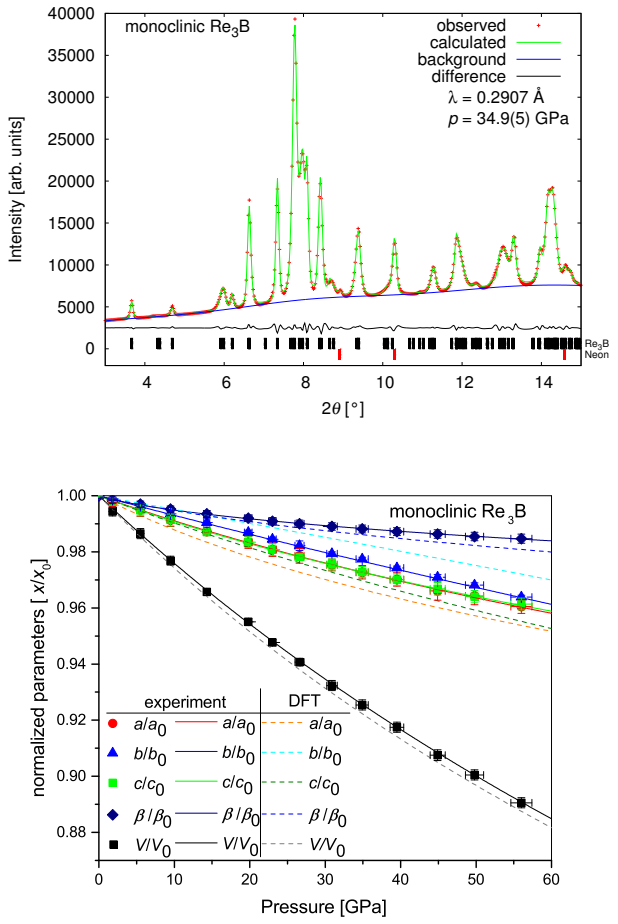

FIG. 8. *Top*: Le Bail refinement of the synchrotron diffraction pattern of monoclinic Re_3B at 34.9(8) GPa. There are no indications of an impurity phase in the small sample area investigated. Diamond reflections were masked before integration of the data. *Bottom*: Pressure dependence of the monoclinic Re_3B lattice parameters up to 56 GPa. Fitting a third order BM equation of state (solid lines) yielded a $B_0 = 390(3)$ GPa and $B_0' = 3.8(2)$. The pressure-induced decrease of the unit cell volume is well described by the DFT calculations, but the experimental compressibilities of the lattice parameters are only in moderate agreement with the DFT data.

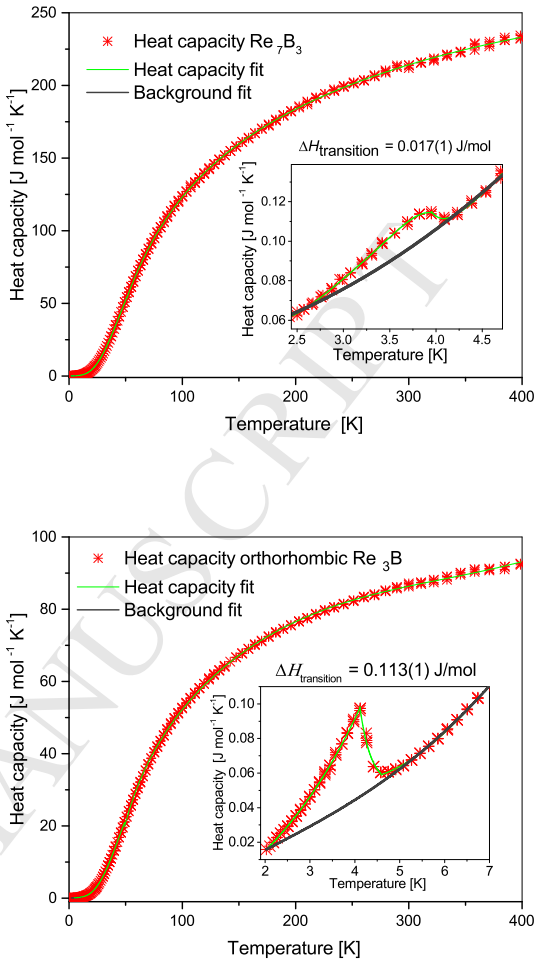

FIG. 9. *Top*: C_p of Re_7B_3 in the temperature range from 1.8 to 395 K obtained by measuring a powder inside a Cu container, whose contribution to the heat capacity was subtracted. The small peak at 3.7 K represents the transition temperature into the superconducting state. *Bottom*: C_p of orthorhombic Re_3B in the same temperature range measured from a polycrystalline solid. The transition is much sharper at a temperature of 4.3 K.

Microcalorimetry

Microcalorimetry was performed on polycrystalline solids from arc-melting (orthorhombic Re_3B) and crushed powders from the samples synthesized in an HF furnace (Re_7B_3). We did not perform measurements on monoclinic Re_3B, since we did not succeed in synthesizing phase pure samples. We also measured elemental Re to evaluate the influence of introducing boron into the structures.

Figure 9 shows the heat capacity of Re_7B_3 and orthorhombic Re_3B. In both data sets a peak at temperatures below 5 K indicates the transition into the superconducting state. The transition temperatures of both orthorhombic Re_3B and Re_7B_3 coincide with the transition temperatures obtained by Kawano *et al.* [24] from resistance and SQUID measurements. The thermodynamic parameters are listed in table VII, together with those of elemental Re and B. The Debye temperatures do not vary much for the two boride phases (329(3) and 320(2) K for Re_7B_3 and orthorhombic Re_3B, respectively) and are higher than for elemental rhenium Re by approximately 10%. On the other hand they are roughly four times lower than for elemental B, which shows a Debye temperature higher than 1200 K [44]. The T^3-plots are shown in figure 10. We did not consider the T^2 behavior, since this would have led to an overestimation of the

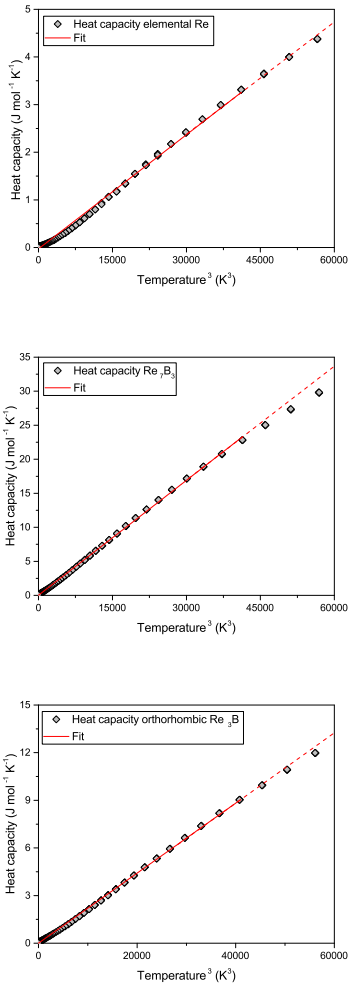

FIG. 10. *Top*: T^3-fit of elemental rhenium. *Middle*: T^3-fit of Re_7B_3. *Bottom*: T^3-fit of orthorhombic Re_3B. In all cases the data was only fitted in the temperature interval between 1.8 an ≈ 34 K and is represented by the solid line. The dashed line represents the extrapolation of the fit.

contribution of the magnetic phase transformation at low temperatures.

Hardness measurements

We performed hardness measurements on Re_7B_3 at two different indentation loads of 5 kgf and 10 kgf on a polycrystalline sample obtained by arc-melting. The analysis of the indentation marks yielded H_V (Re_7B_3, 5 kgf) = 14.5(4) GPa and H_V (Re_7B_3, 10 kgf) = 14.1(3) GPa. However, the values are indicative only as the Re_7B_3 sample obtained by arc melting contained minor impurities of ReB_2.

DFT calculations

The DFT-based calculations reproduced the structure and compressibility of Re_7B_3 very satisfactory (table III, figure 6). The results of the elastic calculations are shown in table VIII. The computed bulk modulus $B_{0,\mathrm{DFT}}$ (Re_7B_3) = 386(1) GPa and B'_{DFT} (Re_7B_3) = 4.4(3) agree very well with the experimental values $B_{0,\mathrm{exp.}}$ (Re_7B_3) = 391(5) GPa, $B'_{\mathrm{exp.}}$ (Re_7B_3) = 4.9(3)). $B_{0,\mathrm{DFT}}$ can also be computed from the elastic stiffness tensor. The corresponding value is $B_{\mathrm{DFT},c_{ij}}$ (Re_7B_3) = 381(1) GPa. The elastic Debye temperature $\theta_{D,\mathrm{DFT,elastic}}$ = 412 K is in moderate agreement to the experimental value ($\theta_{D,\mathrm{exp.}}$ = 320(2) K). The theoretical shear modulus G_{DFT} (Re_7B_3) = 148 GPa and the theoretical Young's modulus Y_{DFT} (Re_7B_3) = 393 GPa agree well in terms of shear and moderately well in terms of Young's modulus with the theoretical values obtained in the study of Juarez-Arellano *et al.* [4] ($G(Re_7B_3)$ = 159 GPa and $Y(Re_7B_3)$ = 466 GPa). The predicted hardness according to the approach presented by Tian *et al.* [47] is 11 GPa, which is about half of the estimate given by Juarez-Arellano *et al.* [4], who used the approach described by Ivanovskii [48] in their calculations.

The ground state structure for orthorhombic Re_3B is well reproduced (table IV). The bulk modulus obtained from theoretical compression data is $B_{0,\mathrm{DFT}}$ (orthorhombic Re_3B) = 389(1) GPa with a B'_{DFT} (orthorhombic Re_3B) = 4.4(3), whereas the experimental values are $B_{0,\ \mathrm{exp.}}$ (orthorhombic Re_3B) = 393(3) GPa with a $B'_{\mathrm{exp.}}$ (orthorhombic Re_3B) = 2.8(2). The bulk modulus from elasticity yields $B_{\mathrm{DFT},c_{ij}}$ (orthorhombic Re_3B) = 327 GPa, which is lower than the experimental and the theoretical values just mentioned. However, in earlier ([4], [49]) and the present study a value c_{44} <0 is obtained. This is unphysical and indicates that the real structure of orthorhombic Re_3B is likely stabilized by defects, such as additional interstitial boron atoms. Specifically, in ideal orthorhombic Re_3B only the prismatically coordinated sites (Wyckoff 4*c*: 0, 0.744, 1/4) are occupied by boron. A hypothetical structure, in which all boron atoms are located on 4*b* (0, 1/2, 0) would have similar lattice parameters and be less stable by ≈ 136 kJ/mol. Hence, given that samples are synthesized at high temperatures, a slight occupation of the 4*b* site can be expected.

In monoclinic Re_3B, there are two sites which can potentially host the boron atoms. The 4*i* site is situated in the center of a trigonal prism (0.744, 0, 0.25) and octahedrally coordinated sites are 2*d* at (0,5, 0, 0.5) and 2*b* at (0, 0.5, 0). DFT calculations show that indeed a structure with all B atoms in the prismatic coordination is more stable by 136 kJ/mol. However, the lattice parameters of a structure in which all octahedra are occupied by boron differs only slightly from the structure with all boron atoms in prismatic coordination, and, given the relatively

TABLE VII. Thermodynamical properties of Re_7B_3, orthorhombic Re_3B, rhenium and boron at 298 K.

Compound		C_p [J/mol K]	ΔH^0_{298} [J/mol]	S^0_{298} [J/mol K]	θ_D [K]
Re elemental	this study	24.67(25)	5196(51)	35.59(34)	292(2) ([45] = 272)
Re_7B_3	this study	210(4)	40558(400)	267(2)	320(2)
Re_3B	this study	86(1)	16950(170)	112(1)	329(3) ([24] = 600)
B elemental	([44],[46])	11.1	1222(8)	5.90(8)	1219

small energy differences caused by placing boron atoms in octahedral coordination the DFT calculations are consistent with a slight disordering or a slight excess of boron at the high temperatures prevalent during synthesis.

The experimental bulk modulus of monoclinic Re_3B is $B_{0,\text{exp.}}$ (monoclinic Re_3B) = 362(1) GPa with $B'_{\text{exp.}}$ (monoclinic Re_3B) = 4.4(3), which is in agreement with the experimental ($B_{0,\text{exp.}}$ (monoclinic Re_3B) = 390(3) GPa with $B'_{\text{exp.}}$ (monoclinic Re_3B) = 3.7(2)) and elastic ($B_{\text{DFT},c_{ij}}$ = 372 GPa) bulk moduli.

The elastic Debye temperatures $\theta_{D,\text{DFT,elastic}}$ (Re_7B_3) = 412 K, $\theta_{D,\text{DFT,elastic}}$ (ReB_2) = 730 K and $\theta_{D,\text{DFT,elastic}}$ ($C2/m$ "$Re_{24}B_8$") = 404 K are in moderate agreement with the experimental value ($\theta_{D,\text{exp.}}$ (Re_7B_3) = 320(2) K. The value obtained for $\theta_{D,\text{DFT,elastic}}$ (ReB_2) = 730 K is much higher than those of the other binary borides and this also holds for the average sound velocity (ν_{average} (ReB_2) = 5121 m/s) and the G_{DFT} and Y_{DFT} moduli. The predicted hardness, which is very high in the case of ReB_2 (H (ReB_2) = 40 GPa) and significantly lower for the more metal rich phases (H (Re_7B_3) = 11 GPa and H (monoclinic Re_3B) = 11 GPa). The theoretical hardness of Re_7B_3 is thus in good agreement to the experimental value of roughly 14 GPa.

TABLE VIII. Bulk modulus B from elasticity, elastic Debye temperature $\theta_{D,\text{elastic}}$, average sound velocity ν_{average}, shear modulus G, Young's modulus Y, Poisson's ratio ν, hardness H and universal anisotropy index A^U. Data for structures with space group symbols $Cmcm$ and $C2/m$ correspond to values computed with supercells.

		Re_7B_3	ReB_2	$Cmcm$ "$Re_{12}B_4$"	$C2/m$ "$Re_{24}B_8$"
B [GPa]	this study, DFT	381(1)	332(4)	327(1)[1]	372(1)
	[4]	385	335	389	-
	[49]	378	348	379	-
	[23]	405	369	-	-
	[43]	380	347	420	-
$\theta_{D,\text{elastic}}$ [K]	this study, DFT	412	730	-	404
	[23]	448	755	-	-
ν_{average} [m/s]	this study, DFT	3161	5121	-	3140
$G^{(2)}$ [GPa]	this study, DFT	148	277	-	150
	[4]	159	283	-	-
	[49]	160	288	-	-
	[23]	148	294	-	-
	[43]	151	276	-	-
$Y^{(2)}$ [GPa]	this study, DFT	393	654	-	397
	[4]	466	599	-	-
	[49]	420	677	-	-
	[23]	395	696	-	-
	[43]	402	654	-	-
$\nu^{(2)}$	this study, DFT	0.33	0.18	-	0.32
	[49]	0.3145	0.1757	-	-
	[23]	0.34	0.19	-	-
	[43]	0.32	0.19	-	-
H [GPa]	this study, exp.	$\approx$ 14(1)[3]	-	-	11
	this study, DFT	11	40[4]	-	11
	[4]	24.1	44.7	-	-
	[48]	-	43	-	-
A^U[5]	this study	0.05	0.25	-	2.8

[1] but $c_{44} \leq 0$
[2] $2G(1+\nu) = Y = 3B(1-2\nu)$ for isotropic materials
[3] 14.5(4) GPa at kgf, 14.1(3) GPa at 10 kgf
[4] $H(ReB_2,\ \text{exp.})$ = 30-48 GPa [50]
[5] $A^U = 5G^V/G^R + B^V/B^R - 6 \geq 0$ (G^V and G^R = Voigt and Reuss estimates of G, B^V and B^R = Voigt and Reuss estimates of B [51])

EELS

The experimentally determined boron K-edge spectra of ReB_2 and orthorhombic Re_3B are displayed in figure 11, where they are compared to the results of the DFT calculations. The agreement between theory and experiment is satisfactory. The main observation is that in Re_3B the K-edge is rather narrow, with a full width at half maximum (FWHM) of $\approx$ 5 eV, while the corresponding edge in ReB_2 is much broader, with a FWHM $\approx$ 10 eV and clearly has several distinct maxima.

This is consistent with the difference in the variations in the environment of the boron atoms. In Re_3B, the boron atoms are only coordinated by rhenium atoms, which are all at very similar distances ($\approx$ 2.2 Å). In contrast, in ReB_2, the situation is more complex, with very strong boron-boron bonds in addition to B-Re bonds. We were unable to observe a spectrum for Re_7B_3 due to difficulties during the preparation of the samples. A spectrum predicted using the DFT calculations is shown in figure 12.

The spectrum seems to represent an intermediate case between the two cases discussed above, and in fact the environment around the boron atoms in Re_7B_3 is slightly more complex than in Re_3B, as there are B-Re bonds ranging from 2.2 - 2.7 Å, while there are no B-B bonds.

CONCLUSIONS AND DISCUSSION

In the present study, we have outlined the conditions allowing the synthesis of binary rhenium borides and, contrary to earlier findings, have shown that monoclinic Re_3B can be obtained at ambient pressures. As monoclinic Re_3B is therefore not a high pressure phase, there is no problem with its molar volume being larger than that of the orthorhombic phase. These experimental findings were confirmed by the DFT calculations, which indicated

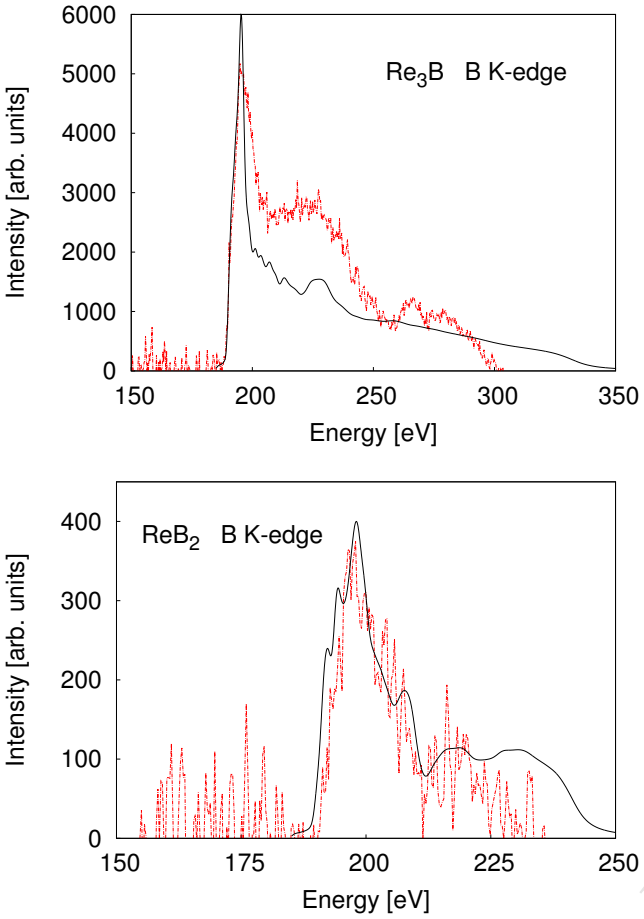

FIG. 11. EEL spectra of orthorhombic Re_3B (top) and ReB_2 (bottom) . The red lines show the measured data, the black ones represent the calculated spectra.

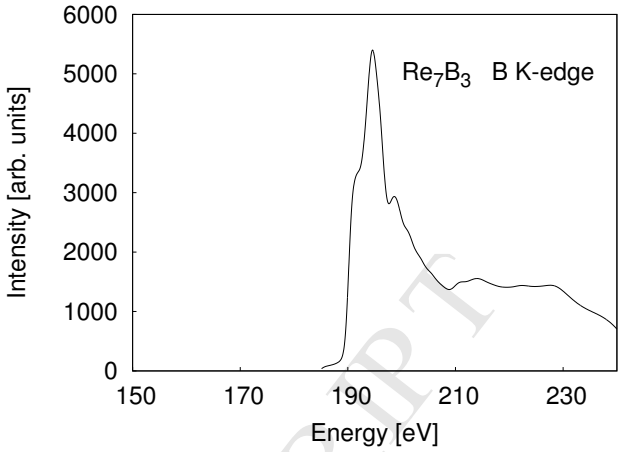

FIG. 12. Theoretical EEL spectrum of Re_7B_3.

that both Re_3B modifications should be (meta-)stable at ambient conditions, shown by negative values for H_f.

Another issue which has been resolved here is the finding, that DFT calculations predict orthorhombic Re_3B to be elastically unstable ($c_{44} \leq 0$), which was also found in two earlier studies ([49], [4]). Calculations based on the monoclinic phase with orthorhombic structures, where in the latter additional boron was incorporated, show that then the structures become elastically stable. For this, the elastic stiffness tensors of several orthorhombic supercells were calculated, in which boron atoms were placed on octahedrally coordinated sites. In all cases, the elastic stiffness tensor then had no negative components. This is consistent with the results of Kayhan [21], who carried out neutron diffraction experiments on the rhenium boride phases Re_7B_3, orthorhombic Re_3B and ReB_2. Kayhan [21] confirmed the structural models reported in the literature, but would not have been able to detect small additional amounts of boron on the other available sites.

The current study also places much better constraints on the elasticity of the binary rhenium borides. Re_7B_3 is less compressible than most of the other metal borides like TaB_2 (341(7) GPa), WB_2 (341-372 GPa), WB_4 (304-325 GPa) or ReB_2 (360-382 GPa) ([50],[52]), but does not reach the ultra-incompressibility of OsB (431-453 GPa) or diamond. Orthorhombic Re_3B on the other hand shows a higher bulk modulus than previously assumed and the experimental value is now in better agreement with theory. One possible explanation for the underestimated bulk modulus in the study of Juarez-Arellano *et al.* [4] might be the presence of monoclinic Re_3B instead of its orthorhombic polymorph, since the monoclinic modification was also reported to form at elevated (p,T)-conditions by Tyutyunnik *et al.* [5]. It would be very challenging to distinguish the two polymorphs with high energy synchrotron radiation in a phase mixture with significant overlapping of reflections.

Another point that prevented a more exact determination of the bulk moduli in the earlier study is the maximum applied pressure of only around 22 GPa. This precludes an accurate determination of the pressure derivative B' more difficult and is thus easily accompanied by larger errors. As a consequence all bulk moduli in the study of Juarez-Arellano *et al.* [4] have been derived using the 2^{nd} order BM eos. In this study we obtained $B'_{\mathrm{exp.}}$ (Re_7B_3) = 4.9(3) and $B'_{\mathrm{exp.}}$ (Re_3B) = 2.8(2) GPa, which derivate from the fixed value of 4, which is used in the 2^{nd} order BM eos.

The DFT compression data for monoclinic Re_3B yielded a smaller B_0 = 362(1) GPa and a B'_0 of 4.4(3) than determined in the experiment. In this case the deviation of B_0 between theory and experiment is more than 7%. This, however, was to be expected, as the DFT calculations were restricted to a structure without any occupation of the $2d$ and $2b$ positions, which are occupied with low probabilities in the actual compound.

All the phases that have been investigated in terms of

their compressibility in this study show higher experimental and theoretical bulk moduli than elemental rhenium, which is 350(15) GPa [53]. Only the value derived by DFT for monoclinic Re_3B coincides with elemental rhenium within the error limits. Hence it is obvious, that the incorporation of boron into the dense metal structures increases the incompressibility of the compounds to a certain extent. Elemental boron on the other hand shows a bulk modulus of only 224(15) GPa [54]. So, we expect borides with higher boron-to-metal-ratios to show smaller bulk moduli, as already stated by Gu *et al.* [1].

In our microcalorimetry experiments we could not reproduce the determined value of a Debye temperature of $\theta_D = 600$ K by Kawano *et al.* [24] for orthorhombic Re_3B, which is almost twice as high as the value obtained in our study. For comparison, the Debye temperature of ReB_2 at 298 K was found to be between 716 and 782 K by experiment and LDA and GGA-calculations ([55], [6], [9], [22], [56]). For the monoclinic modification of Re_3B, we do not expect major changes in the thermodynamic values and they should be very similar to the one obtained for the orthorhombic modification.

Indentation measurements on Re_7B_3 revealed a hardness which is in satisfactory agreement with theory. This supports the underlying assumptions of the approach we used in our calculations. It is worthwhile to mention that the presence of ReB_2 as an impurity phase in the specimen employed for hardness testing might have shifted the result to a slightly higher value, since ReB_2 is known to have a high hardness (30-48 GPa [50]) both from experimental and theoretical considerations. The hardness obtained here is thought to be more reliable than the results of calculations carried out by Juarez-Arellano *et al.* [4], where an empirical approach yielded a significantly higher value for Re_7B_3 of 24.1 GPa.

The calculated elastic properties for monoclinic Re_3B are consistent with the results for the other rhenium borides. The hardness and the elastic moduli are closer to the ones for Re_7B_3 than for the orthorhombic modification. This might be attributed to the fact that the calculations were performed under the supposition that the $2d$ and $2b$ positions were fully occupied and covalent bonding becomes more dominant than in orthorhombic Re_3B, which could explain the higher elastic moduli and the higher hardness predicted from theory.

The results of our EELS measurements and the corresponding DFT calculations imply that EELS can efficiently be used to distinguish between local environments of boron atoms, and hence, in combination with DFT, can be used to confirm structural models for the location of a very light element in the presence of very heavy elements without having to use neutron diffraction, which requires a substantial amount of sample enriched with ^{11}B.

Acknowledgments

C. Neun thanks Dr. Alexandra Friedrich (Universitity of Würzburg, Germany) for her support and help during beamtimes at P02.2/PETRA III and Dr. Norimasa Nishiyama (Deutsches Elektronen-Synchrotron, Hamburg - now: Tokyo Institute of Technology, Japan) for carrying out the hardness measurements. Also we want to acknowledge Dominik Zimmer for his help during sample preparation. We gratefully acknowledge the DFG (project 1232-401-1) for funding in the framework of an ERA-chemistry project and so is the FWF (I-1636-N19). Furthermore we thank the BMBF (project 05K13RF1 and 05K16RFB) and the Conacyt (grant FC-2015-2-947) for funding. The Hermann Willkomm-Stiftung in Frankfurt is also acknowledged for providing travel grants. F. Schmuck and D. Spahr are grateful for financial support by the German Academic Exchange Service (DAAD). We thank LINAN for access to electron microscopy facilities and I. Becerril and A. I. Peña for technical support at the IPICyT.

* **Corresponding author**:
Christopher Neun
Institute of Geoscience
Crystallography
Altenhöferallee 1
60438 Frankfurt am Main, Germany
neun@kristall.uni-frankfurt.de

[1] Q. Gu, G. Krauss, and W. Steurer, Advanced Materials **20**, 3620 (2008).
[2] ICSD, ICSD Release 2016/2, Fachinformationszentrum Karlsruhe (2016).
[3] R. B. Kaner, J. J. Gilman, and S. H. Tolbert, Science **308**, 1268 (2005).
[4] E. A. Juarez-Arellano, B. Winkler, A. Friedrich, L. Bayarjargal, W. Morgenroth, M. Kunz, and V. Milman, Solid State Sciences **25**, 85 (2013).
[5] A. Tyutyunnik, T. Dyachkova, Y. Zaynulin, and S. Gromilov, Journal of Structural Chemistry **55**, 84 (2014).
[6] Y. Wang, J. Zhang, L. L. Daemen, Z. Lin, Y. Zhao, and L. Wang, Physical Review B **78**, 224106 (2008).
[7] H.-Y. Chung, M. B. Weinberger, J. B. Levine, A. Kavner, J.-M. Yang, S. H. Tolbert, and R. B. Kaner, Science **316**, 436 (2007).
[8] X.-Q. Chen, C. L. Fu, M. Krčmar, and G. S. Painter, Phys. Rev. Lett. **100**, 196403 (2008).
[9] Y. Liang and B. Zhang, Physical Review B **76**, 132101 (2007).
[10] F. Peng, Q. Liu, H. Fu, and X. Yang, Solid State Communications **149**, 56 (2009).
[11] A. Simunek, Physical Review B **80**, 060103 (2009).
[12] C. Zang, H. Sun, J. S. Tse, and C. Chen, Physical Review B **86**, 014108 (2012).

[13] B. Aronsson, E. Stenberg, and J. Aselius, Acta Chemica Scandinavica **14**, 733 (1960).

[14] B. Aronsson, M. Backman, and S. Rundqvist, Acta Chemica Scandinavica **14**, 1001 (1960).

[15] N. Dubrovinskaia, L. Dubrovinsky, and V. L. Solozhenko, Science **318**, 1550c (2007).

[16] S. Otani, T. Aizawa, and Y. Ishizawa, Journal of Alloys and Compounds **252**, L19 (1997).

[17] M. Frotscher, M. Hölzel, and B. Albert, Zeitschrift für anorganische und allgemeine Chemie **636**, 1783 (2010).

[18] S. Guo, Journal of the European Ceramic Society **34**, 4443 (2014).

[19] H. Takagiwa, A. Kawano, Y. Mizuta, T. Yamamoto, M. Yamada, K. Ohishi, T. Muranaka, J. Akimitsu, W. Higemoto, and R. Kadono, Physica B: Condensed Matter **326**, 355 (2003).

[20] G. Strukova, V. Degtyareva, D. Shovkun, V. Zverev, V. Kiiko, A. Ionov, and A. Chaika, arXiv preprint cond-mat/0105293 (2001).

[21] M. Kayhan, *Transition Metal Borides: Synthesis, Characterization and Superconducting Properties*, Ph.D. thesis, Technische Universität Darmstadt (2013).

[22] X. Hao, Y. Xu, Z. Wu, D. Zhou, X. Liu, X. Cao, and J. Meng, Physical Review B **74**, 224112 (2006).

[23] E. Zhao, J. Wang, J. Meng, and Z. Wu, Journal of Computational Chemistry **31**, 1904 (2010).

[24] A. Kawano, Y. Mizuta, H. Takagiwa, T. Muranaka, and J. Akimitsu, Journal of the Physical Society of Japan **72**, 1724 (2003), http://dx.doi.org/10.1143/JPSJ.72.1724.

[25] H. Huppertz, Zeitschrift für Kristallographie-Crystalline Materials **219**, 330 (2004).

[26] D. Walker, M. Carpenter, and C. Hitch, American mineralogist **75**, 1020 (1990).

[27] A. C. Larson and R. B. Von Dreele, LANSCE, MS-H805, Los Alamos, New Mexico (1994).

[28] B. H. Toby, Journal of Applied Crystallography **34**, 210 (2001).

[29] A. Bruker, *TOPAS V3: General profile and structure analysis software for powder diffraction data, User's Manual* (Bruker AXS, Karlsruhe, Germany, 2005).

[30] R. Boehler, Review of Scientific Instruments **77**, 115103 (2006).

[31] H. Mao, P. Bell, J. T. Shaner, and D. Steinberg, Journal of Applied Physics **49**, 3276 (1978).

[32] A. Hammersley, European Synchrotron Radiation Facility Internal Report ESRF97HA02T **68** (1997).

[33] C. Prescher and V. B. Prakapenka, High Pressure Research **35**, 223 (2015).

[34] F. Murnaghan, Proceedings of the National Academy of Sciences **30**, 244 (1944).

[35] F. Birch, Phys. Rev. **71**, 809 (1947).

[36] R. J. Angel, M. Alvaro, and J. Gonzalez-Platas, Zeitschrift für Kristallographie-Crystalline Materials **229**, 405 (2014).

[37] J. Lashley, M. Hundley, A. Migliori, J. Sarrao, P. Pagliuso, T. Darling, M. Jaime, J. Cooley, W. Hults, L. Morales, *et al.*, Cryogenics **43**, 369 (2003).

[38] Q. Design, 11578 Sorrento Valley Road, San Diego, CA 29121 (http://www.qdusa.com).

[39] J. Lashley, M. Hundley, A. Migliori, J. Sarrao, P. Pagliuso, T. Darling, M. Jaime, J. Cooley, W. Hults, L. Morales, D. Thoma, J. Smith, J. Boerio-Goates, B. Woodfield, G. Stewart, R. Fisher, and N. Phillips, Cryogenics **43**, 369 (2003).

[40] H. Carslaw and J. Jaeger, *Heat in solids*, Vol. 1 (Clarendon Press, Oxford, 1959).

[41] S. J. Clark, M. D. Segall, C. J. Pickard, P. J. Hasnip, M. I. Probert, K. Refson, and M. C. Payne, Zeitschrift für Kristallographie **220**, 567 (2005).

[42] Z. Wu and R. E. Cohen, Physical Review B **73**, 235116 (2006).

[43] X. Zhao, M. C. Nguyen, C.-Z. Wang, and K.-M. Ho, Journal of Physics: Condensed Matter **26**, 455401 (2014).

[44] J. C. Thompson and W. J. McDonald, Physical Review **132**, 82 (1963).

[45] C. Y. Ho, R. W. Powell, and P. E. Liley, *Thermal conductivity of the elements: a comprehensive review*, Tech. Rep. (DTIC Document, 1974).

[46] J. Cox, D. D. Wagman, and V. A. Medvedev, *CODATA key values for thermodynamics* (Chem/Mats-Sci/E, 1989).

[47] Y. Tian, B. Xu, and Z. Zhao, International Journal of Refractory Metals and Hard Materials **33**, 93 (2012).

[48] A. Ivanovskii, Journal of Superhard Materials **34**, 75 (2012).

[49] H. Gou, Z. Wang, J. Zhang, S. Yan, and F. Gao, Inorganic chemistry **48**, 581 (2008).

[50] A. Friedrich, B. Winkler, E. A. Juarez-Arellano, and L. Bayarjargal, Materials **4**, 1648 (2011).

[51] S. I. Ranganathan and M. Ostoja-Starzewski, Physical Review Letters **101**, 055504 (2008).

[52] B. Winkler, E. A. Juarez-Arellano, A. Friedrich, L. Bayarjargal, F. Schröder, J. Biehler, V. Milman, S. M. Clark, and J. Yan, Solid State Sciences **12**, 2059 (2010).

[53] L.-G. Liu, T. Takahashi, and W. A. Bassett, Journal of Physics and Chemistry of Solids **31**, 1345 (1970).

[54] R. J. Nelmes, J. S. Loveday, D. R. Allan, J. M. Besson, G. Hamel, P. Grima, and S. Hull, Physical Review B **47**, 7668 (1993).

[55] M. R. Koehler, V. Keppens, B. C. Sales, R. Jin, and D. Mandrus, Journal of Physics D: Applied Physics **42**, 095414 (2009).

[56] W. Zhou, H. Wu, and T. Yildirim, Physical Review B **76**, 184113 (2007).

Highlights

- All known binary rhenium boride phases can be synthesized at ambient pressure
- All phases are very incompressible
- A full set of thermodynamic values was obtained
- EELS can be employed to confirm structural models of borides
- Elastic properties have been calculated for the binary rhenium boride phases